RESEARCH ARTICLE | FEBRUARY 09 2024

Electron transfer in a crystalline cytochrome with four hemes

William W. Parson ; Jingcheng Huang ; Martin Kulke ; Josh V. Vermaas ; David M. Kramer

J. Chem. Phys. 160, 065101 (2024)
https://doi.org/10.1063/5.0186958
CHORUS

The Journal of Chemical Physics ARTICLE pubs.aip.org/aip/jcp

Electron transfer in a crystalline cytochrome with four hemes

Cite as: J. Chem. Phys. 160, 065101 (2024); doi: 10.1063/5.0186958
Submitted: 9 November 2023 • Accepted: 18 January 2024 •
Published Online: 9 February 2024

William W. Parson,[1,a)] Jingcheng Huang,[2] Martin Kulke,[2,b)] Josh V. Vermaas,[2] and David M. Kramer[2,c)]

AFFILIATIONS

[1] Department of Biochemistry, University of Washington, Seattle, Washington 98195, USA
[2] DOE-Plant Research Laboratory and Department of Biochemistry and Molecular Biology, Michigan State University, East Lansing, Michigan 48824, USA

[a)] **Author to whom correspondence should be addressed:** parsonb@u.washington.edu
[b)] **Current address:** Center for Functional Protein Assemblies, Technical University of Munich, Ernst-Otto-Fischer Str. 8, 85748, Garching, Germany
[c)] **Current address:** Jan IngenHousz Institute, Wageningen, The Netherlands

ABSTRACT

Diffusion of electrons over distances on the order of 100 μm has been observed in crystals of a small tetraheme cytochrome (STC) from *Shewanella oneidensis* [J. Huang *et al.* J. Am. Chem. Soc. **142**, 10459–10467 (2020)]. Electron transfer between hemes in adjacent subunits of the crystal is slower and more strongly dependent on temperature than had been expected based on semiclassical electron-transfer theory. We here explore explanations for these findings by molecular-dynamics simulations of crystalline and monomeric STC. New procedures are developed for including time-dependent quantum mechanical energy differences in the gap between the energies of the reactant and product states and for evaluating fluctuations of the electronic-interaction matrix element that couples the two hemes. Rate constants for electron transfer are calculated from the time- and temperature-dependent energy gaps, coupling factors, and Franck–Condon-weighted densities of states using an expression with no freely adjustable parameters. Back reactions are considered, as are the effects of various protonation states of the carboxyl groups on the heme side chains. Interactions with water are found to dominate the fluctuations of the energy gap between the reactant and product states. The calculated rate constant for electron transfer from heme IV to heme I*b* in a neighboring subunit at 300 K agrees well with the measured value. However, the calculated activation energy of the reaction in the crystal is considerably smaller than observed. We suggest two possible explanations for this discrepancy. The calculated rate constant for transfer from heme I to II within the same subunit of the crystal is about one-third that for monomeric STC in solution.

I. INTRODUCTION

Living things have evolved ways to capture energy released by electron transfer between a great variety of oxidants and reductants. Bacteria of the genera *Shewanella* and *Geobacter* use extended arrays of proteins containing multiple hemes or other electron carriers to shuttle electrons from intracellular substrates to insoluble extracellular acceptors, such as Fe(III) and Mn(IV) oxides.[1–9] These reactions cover distances on the order of 100 μm, traversing the cell membrane, periplasm, and outer membrane. They require electrons to negotiate both exergonic and endergonic steps and to hop from protein to protein as well as between the carriers within each protein. Huang *et al.*[10] have probed electron transfer between the protein subunits of crystals of the small tetraheme cytochrome (STC) of *S. oneidensis* (Fig. 1) by reducing hemes on one edge of the crystal photochemically and measuring the rate at which a zone of reduction diffuses across the crystal. This work provided a dramatic demonstration of electron transfer over macroscopic distances.

While exciting, the results were not easy to reconcile with existing electron-transfer theory. The rate-limiting endoergic step of electron transfer from heme IV in one subunit to heme I*b* in the neighboring subunit had an unexpectedly large activation energy of about 0.43 eV and was considerably slower than had been anticipated on the basis of semiclassical electron-transfer theory. The

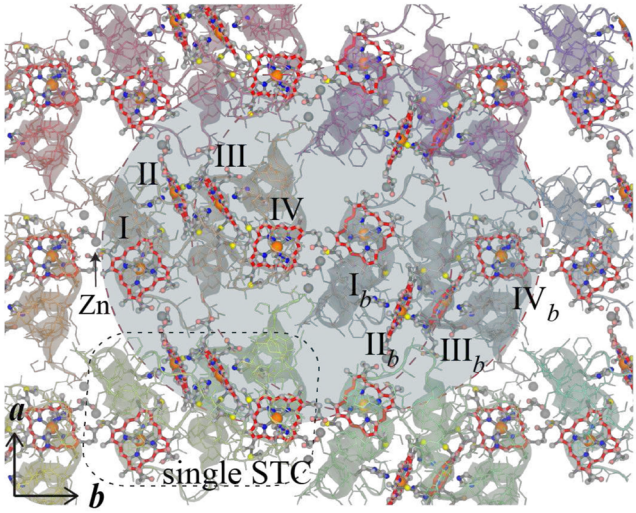

FIG. 1. Structure of crystalline STC[10] viewed along the crystallographic *c* axis. Hemes are represented as ball-and-stick models with Fe atoms in *orange* and the porphyrin rings outlined in *red*. The four hemes of one subunit are labeled I–IV, and those of the neighboring subunit on the positive *b* axis are labeled I*b*–IV*b*. The protein is represented with lines and ribbons in a different color for each subunit. The *black dashed line* indicates an individual subunit (*single STC*). Zn ions (*Zn*) are shown as *gray spheres*. Hydrogens and water molecules are omitted for clarity. Redox titrations of the hemes[10,14,15] suggest that the rate of electron diffusion along the *b* axis is limited by endergonic jumps from heme IV to heme I*b*. The area shaded in *light blue* indicates the union of spheres with radii of 25 Å centered on these hemes.

large activation energy, together with other instances where existing theory fits poorly with experimental findings,[11–13] raised several interesting questions. Does electron-transfer in protein crystals differ from that in solution in any fundamental respects? Or do the differences between the expected and observed rates expose shortcomings of the semiclassical electron-transfer theory? In the first case, understanding the kinetics in crystals could provide insights into the operation of bacterial molecular wires and perhaps help to inform design of synthetic systems for moving electrons over long distances. In the second, it could aid progress toward an improved theory with fewer fitting parameters. These possibilities, of course, are not mutually exclusive.

Extended molecular-dynamics (MD) simulations by Kulke *et al.*[16] based on the same crystal structure argue against the possibility that the distribution of distances between subunits in the crystal changes significantly between 270 and 310 K, the temperature range over which the activation energy was measured. In the present work, we investigate the dynamics of electron transfer in crystalline and monomeric STC by MD simulations with an approach that goes beyond the semiclassical Marcus expression by including changes in entropy. The treatment considers the fluctuating electrostatic energies and electronic coupling factors and the Franck–Condon-weighted density of states for electron transfer between hemes. We also consider the possible importance of differences between the quantum mechanical energies of the electron donor and acceptor hemes and of the protonation states of the carboxyl groups in the propionyl side chains of the hemes.

II. METHODS

A. Electron-transfer rate constants

The rate constant for an electron-transfer reaction (k_{et}) depends on four functions of temperature: ΔE, H, ξ, and ρ_{FC}. The first of these, $\Delta E(t, T)$, is the gap between the electronic energies of the reactant and product states at temperature T, which typically fluctuates rapidly with time (t); $H(t, T)$ is the fluctuating electronic-interaction matrix element that couples the two states; and $\xi(t, T)$ is an overall rate constant for relaxations that dissipate energy to the surroundings. The fourth function, $\rho_{FC}(\Delta E, T)$, is the Franck–Condon-weighted density of possible transitions between various vibrational levels of the reactant and product states, which is relatively independent of time but depends on the energy gap as well as temperature. Combining these functions gives a very general expression for any system that is at thermal equilibrium in the reactant state,[17,18]

$$k_{et}(T) = \lim_{\zeta\to\infty}\left\langle \frac{2\pi}{\hbar}|H(t,T)|^2 \times \frac{\hbar\xi(\Delta E(t,T))/2\pi}{|H(t,T)|^2 + \hbar\xi(\Delta E(t,T))/2\pi}\rho_{FC}\left(\Delta E(t,T)\right)\right\rangle_\zeta. \quad (1)$$

Here, $\langle\cdots\rangle_\zeta$ denotes an average over a time period of length ζ. Equation (1) is the same as Eq. (25) of Ref. 17 except that ΔE and ρ_{FC} are written as functions of T in addition to t and the dependence on the length of the trajectory is stated explicitly. The expression is given in a slightly different form as Eq. (7) of Ref. 18, where work underlying it is discussed in more detail and the effective decay rate constant ξ is written as a sum of microscopic decay constants for transitions between different vibrational levels.

In the limit of weak coupling between the reactant and product states, when $\langle|H(t,T)|^2\rangle \ll \langle\hbar\xi(\Delta E(t,T))/2\pi\rangle$, Eq. (1) reduces to the golden-rule expression,

$$k_{et}(T) = \lim_{\zeta\to\infty}\left\langle \frac{2\pi}{\hbar}|H(t,T)|^2\rho_{FC}\left(\Delta E(t,T)\right)\right\rangle_\zeta. \quad (2)$$

The rate constant then quadratically depends on $|H(t, T)|$. In the opposite extreme that $\langle|H(t,T)|^2\rangle \gg \langle\hbar\xi(\Delta E(t,T))/2\pi\rangle$, Eq. (1) goes to the adiabatic limit,

$$k_{et}(T) = \lim_{\zeta\to\infty}\left\langle \xi(t,T)\rho_{FC}\left(\Delta E(t,T)\right)\right\rangle_\zeta, \quad (3)$$

where the rate constant becomes independent of $|H(t, T)|$ but increases with ξ. The relaxation rate constant ξ depends on the number of vibrational normal modes that contribute to ρ_{FC} and increases as ΔE becomes more negative.[18] However, it generally appears to be large enough to make Eq. (2) reliable even for systems with only six to eight normal modes, as long as $|H|$ is less than about 400 cm^{-1} (50 meV).[18] The calculated values of $|H|$ presented below for STC are in this range.

Equation (1) does not assume that the probability of finding a given value of $\Delta E(t, T)$ is a Gaussian, or any other particular function of ΔE, making it applicable to systems with rugged potential-energy surfaces. Unlike the semiclassical Marcus expression,[19–23] which neglects changes in entropy, Eq. (1) avoids the assumption that the variance of $\Delta E(t, T)$ is directly proportional to T. It also does not

make any assumptions about relaxations of ΔE that follow electron transfer, other than that the system dissipates energy with the effective rate constant ξ. Structural rearrangements that occur on longer time scales are irrelevant. Because the treatment does not depend on the reorganization free energy of the reaction, there is no need to evaluate ΔE during a trajectory in the product state unless one also seeks the rate constant for a reaction in the opposite direction. Because Eq. (1) uses the time-dependent functions $\Delta E(t, T)$ and $|H(t, T)|$ rather than average values of ΔE and $|H|$, it is suitable for systems in which the fluctuations of these functions are correlated. If $\langle |H|^2/\hbar\xi \rangle$ is small enough for Eq. (2) to hold, as the results presented below indicate to be the case in STC, the treatment has no adjustable parameters beyond those of the MD simulations and the expressions used for H and ΔE. Those parameters have been optimized in previous studies of other systems and are used here without modifications except as noted below for the equilibrium Fe–N bond lengths.

B. Models

We now describe MD simulations and procedures we used to evaluate $\Delta E(t, T)$, $H(t, T)$, and $\rho_{FC}(t, T)$ for electron-transfer in crystalline and monomeric STC. Models of *S. oneidensis* STC first were constructed from the structure of described by Huang *et al.* (Protein Data Bank ID 6EE7.PDB),[10] in which three Zn ions accompany each protein subunit. (Leys *et al.*[24] have reported on other crystal forms with different packing of the subunits and bound sulfate ions but very similar protein structures.) The models were centered midway between the two hemes for a particular reaction. They were trimmed to remove residues that had no atoms within 25 Å of the Fe atom of either heme, as indicated by the light-blue area in Fig. 1 for hemes IV and I*b*. The trimmed models then were embedded in a bath of flexible, three-point water molecules[25] to fill a sphere with a radius of 32 Å. The model for electron-transfer from heme IV to I*b* in the crystal had 3646 molecules of water and that for transfer from heme I to II had 4102. A similarly constructed model for electron transfer from heme I to II in monomeric STC had 4384 waters. No attempt was made to correct for thermal expansion in any of the models.

C. Molecular-dynamics simulations

MD trajectories were propagated in 1 fs steps using the classical ENZYMIX force field[26,27] with modified van der Waals parameters for water.[17] After Monte Carlo rotations of the water molecules with simulated annealing from 420 to 30 K to minimize the energy, the system was equilibrated by 10 ps MD trajectories at 30 and 200 K and 1 ns at 300 K. Trajectories then were continued for an additional 10 ns at 300 K. Velocity rescaling was used to maintain constant temperature, and the forces on water atoms were rescaled on each step to maintain zero angular momentum. Structures were saved at intervals of 100 fs for calculations of energy gaps and coupling factors. We also carried out trajectories at 10 K intervals between 270 and 340 K; these were propagated for 5 ns following an equilibration period of 100 ps at each temperature.

Atomic charges of the hemes and their attached histidine and cysteine residues were taken from the work of Oliveira *et al.*[28] with minor adjustments to distribute the charges of methyl and methylene groups between the carbons and hydrogens (supplementary material, Table S1). Zn ions were assigned charges of +2, and ionizable amino acid residues were given their canonical charges of ±1 at pH 8. The C-terminal lysine carboxyl group, which binds to one of the Zn ions, was also assigned a charge of −1. For the monomeric protein in solution, nuclear magnetic resonance (NMR) measurements and continuum electrostatics calculations[15,29] are in accord with these assignments of protonation states for the ionizable residues at pH 8, and many of these residues clearly form ion pairs in the crystal structure.[10] The propionyl carboxyl groups of the hemes, however, have pK_as on the order of 7 for STC in solution,[15] making their protonation states in the crystal difficult to predict. We treated all these groups as neutral during the MD trajectories unless they had an oxygen within 3 Å of a Zn^{+2} or a positively charged amino acid group. In this default protonation state, both carboxyl groups of hemes I, I*b*, III, and III*b* and the carboxyl groups on ring A of hemes II and II*b* and ring D of heme IV were neutral, while those on ring D of hemes II and II*b* and ring A of heme IV were negatively charged. The carboxyl groups of hemes II and IV both have Zn^{+2} ions in close proximity (see Figs. S1 and S2). The arrangements of the oxygens of heme II with respect to the Zn^{+2} in the crystal structure[10] suggest that the propionyl side chain of porphyrin ring D is deprotonated but that the propionyl group of porphyrin ring A is not. In heme IV, the arrangements of the oxygens suggest that the propionyl side chain of ring A is deprotonated, while that of ring D is less likely to be. Other possible protonation states were considered when we calculated redox energies.

No counterions were added to the models. Other investigators[23,30,31] have found that adding counterions does not improve calculations of electrostatic energies in proteins that are well solvated with water, and our experience has been similar.

Protein groups and Zn ions whose positions in the crystal structure were more than 25 Å beyond the center of the model were held fixed at those locations during the MD trajectories but were included in calculations of electrostatic interactions. In addition, a quadratic potential with the relatively weak force constant of 10 kcal mol^{-1} $Å^{-2}$ was used to keep the nitrogen atoms of the hemes near their crystallographic positions. The purpose of this constraint was to reduce artefactual drift of the trimmed structures, allowing for more meaningful comparisons of electrostatic interactions of the different hemes with their surroundings. The same constraint was applied in MD simulations of the monomeric protein. Although the constraint could limit fluctuations of the structure and reorganization when a heme is reduced, comparisons of crystal structures of oxidized and reduced STC have shown that full reduction causes no significant changes in the geometry of the heme cluster.[24] In previous MD simulations of STC in solution, Oliveira *et al.*[28] found that full reduction led to movements of backbone atoms at the N-terminus and in two exposed loops of the protein, but again very little change in the heme cluster. No constraints were put on other atoms of the hemes or their histidyl ligands in the crystal. Equilibrium Fe–N bond lengths for the MD force field were obtained by optimizing the structures of model ferrous and ferric bis-imidazole hemes as described below and are given in Table S2.

D. Redox energies

The change in electronic energy (ΔE) when an electron moves between two hemes ($h1$ and $h2$) can be divided into the change in the internal quantum mechanical energy of the hemes and their HIS and

CYS ligands ($\Delta\varepsilon$) and the change in electrostatic interactions with the surroundings (ΔE_s), which can be approximated well classically.[32] We wrote the latter term as

$$\Delta E_s = \sum_h \sum_i (Q_{i,h,P} - Q_{i,h,R}) \sum_j q_j / f_{i,j} r_{i,j} + \sum_{i1} \sum_{i2} (Q_{i1,h1,P} Q_{i2,h2,P} - Q_{i1,h1,R} Q_{i2,h2,R}) / f_{i1,i2} r_{i1,i2}. \quad (4)$$

Index h in the first sum here denotes one of the reacting hemes ($h1$ or $h2$); $Q_{i,h,R}$ is the charge of atom i of reacting heme h and its ligands in the reactant state (electron donor reduced and acceptor oxidized), and $Q_{i,h,P}$ is the corresponding charge in the product (donor oxidized and acceptor reduced); q_j is the charge of atom j of the surrounding protein, water, Zn^{2+} ions, and the hemes other than h; $r_{i,j}$ is the distance between atoms i and j; and f_{ij} is a distance-dependent effective dielectric screening factor. Interactions between atoms connected by less than three bonds were considered to contribute to $\Delta\varepsilon$ and were omitted from the sums in Eq. (4). The atoms of the propionyl side chains of heme h were treated as part of the surroundings along with those of the other hemes in the sum over j. Subscripts $i1$ and $i2$ in the second line denote atoms of the two reacting hemes ($i1$ in heme $h1$, $i2$ in $h2$). Equation (4) assumes that the atomic charges $Q_{i,h,R}$ and $Q_{i,h,P}$ do not fluctuate significantly with time as long as heme h remains in the same redox state.

We used the following expression[33–35] for the dielectric screening factor:

$$f_{ij} = 1 + 60[1 - \exp(-\eta r_{ij})] \quad (5)$$

with $\eta = 1.5$ Å^{-1}. This expression was found to account well for effects of mutations of ionizable amino acid residues in photosynthetic reaction centers, with values of η of either 1.0 or 1.8 Å^{-1} giving essentially the same agreement between calculated and measured changes in the redox potential of the special pair of bacteriochlorophylls.[34] However, it has not previously been used for crystalline proteins or for calculations of electrostatic interactions on very short time scales.

We also calculated ΔE_s with an iterative treatment of induced electric dipoles[17] instead of the dielectric screening factor of Eqs. (4) and (5). The energy gaps calculated with this treatment had similar mean values ($\langle\Delta E\rangle$) but larger variances (σ^2), possibly because they were more sensitive to interactions of the hemes with residues on the edges of the models, where the protein structures and water molecules might undergo artifactually large fluctuations. The distance-dependent screening factor f_{ij} attenuates contributions from these long-range interactions and therefore could give more meaningful results despite its less compelling theoretical justification. We therefore used Eqs. (4) and (5) for all the work presented below.

The charges assigned to the propionyl side chains of the hemes have significant effects on the calculated values of ΔE_s. We therefore calculated ΔE_s for STC in a variety of possible protonation states. The propionyl carboxyl groups of heme I, for example, are protonated in the default state described above for the MD trajectories but project into an aqueous region where an anionic carboxylate would be well solvated, suggesting that one or both carboxyl groups are deprotonated. Both carboxyl groups of heme III are also well solvated.

The quantum mechanical energy difference $\Delta\varepsilon$ varies from one pair of hemes to another and fluctuates with time depending on structural details, such as the positions of the axial histidyl ligands. To relate $\Delta\varepsilon$ to structural parameters that could be calculated efficiently for a large number of structures saved during MD simulations, we evaluated the quantum mechanical energy differences between oxidized and reduced states of a set of 100 hemes from crystal structures of 4-and 6-heme *c*-type cytochromes of *S. oneidensis*,[10,24] *S. frigidmarina*,[36] *Desulforibrio desulfuricans*,[37,38] and *D. vulgaris*[39] and the three central subunits of a cryo-EM structure of OmcS from *Geobacter sulfurreducens*.[40] The HIS and CYS residues attached to the hemes were truncated to methyl-imidazole and methylsulfide. Figure S3 shows the structures of representative trimmed complexes. After the addition of hydrogens at standard positions, energies for the ferrous (singlet spin) and ferric (doublet) states of the trimmed structures *in vacuo* were calculated with GAUSSIAN 16.1[41] using the B3LYP DFT functional with the Def2TZV basis function for Fe and the G6-31(d) basis for all other atoms. The mean energy of the reduced states was 6.176 eV below that of the oxidized states with a standard deviation of ±0.409 eV, which is comparable to the adiabatic electron affinity of 5.17 eV that Smith *et al.*[42] calculated for a model bis(histidine) heme complex.

On the assumption that the surroundings affect $\Delta\varepsilon$ mainly by modifying the structures of the heme-ligand complexes, we sought to express the quantum mechanical energy difference for reducing a given heme (ε^k_{red} for heme k in the set) as a linear function of a tractable number (N) of structural parameters (P^k_i). The coefficients (C_i) for various sets of potentially important parameters were obtained by singular-value decomposition of the simultaneous equations, $\varepsilon^k_{red} = \sum_{i=1}^{N} C_i P^k_i$. The quantum-mechanical term $\Delta\varepsilon$ for electron transfer in a given MD structure then was written as the difference between the values of ε^k_{red} for the electron acceptor and donor hemes: $\Delta\varepsilon = \varepsilon^{acceptor}_{red} - \varepsilon^{donor}_{red}$. The most pertinent parameters proved to be the mean distances from the Fe to HIS NE2 atoms and the N atoms of the porphyrin ring. A combination of these distances with two minor parameters and a constant term sufficed to fit the values of ε^k_{red} for the 100 structures with a reduced χ^2 (mean squared deviation) of 0.153 (Table I). We also evaluated lengths of the porphyrin–cysteinyl C–S bonds, asymmetry of pyrrole rings A and C relative to B and D, and tilting of the one imidazole ring relative to the other, but these parameters did not improve χ^2 sufficiently to warrant including.

E. Franck–Condon-weighted density of states

Normal-mode vibrational frequencies and vectors were calculated with GAUSSIAN 16.1[41] for a model six-coordinate heme, *bis*(imidazole)-iron-octamethylporphyrin (Fig. S4). The structures of the reduced and oxidized molecules were optimized with the B3LYP DFT functional using the Def2TZV basis function for Fe and the G6-31(d) basis for all other atoms as in the treatment of $\Delta\varepsilon$ described above. Spectra of Franck–Condon-weighted density of vibrational states (FCWDS) for oxidation or reduction of the model compound then were calculated with the program MolFC3,[43–45] which considers Duschinsky effects and changes in vibrational

TABLE I. Structural parameters and coefficients for $\Delta\varepsilon$.

Parameter	Definition	$\langle P_i \rangle \pm \sigma$[a]	C_i[b]	$C_i \langle P_i \rangle$[c]
1	Mean distance from Fe to a HIS NE2 atom.	2.0198 ± 0.0428 Å	1.7774 eV/Å	3.5900 eV
2	Mean distance from Fe to heme N atoms NA, NB, NC, and ND.	2.0289 ± 0.0336 Å	−1.1692 eV/Å	−2.3722 eV
3	Minimum of cos(θ) and 1.0 − cos(θ), where θ is the angle between the CG1 → CD2 vectors of the two histidines.	0.1518 ± 0.0713	−0.7085 eV	−0.1076 eV
4	Difference between the distances from Fe to NE2 in the two hemes.	0.0229 ± 0.0228 Å	2.8980 eV/Å	0.0646 eV
Constant	1.0	1.0	−7.3533 eV	−7.3533 eV
Sum				−6.1761 eV

[a]Mean ($\langle P_i \rangle$) and standard deviation (σ) of parameter P_i in the set of 100 heme structures.
[b]Coefficient for parameter P_i in the linear combination $\varepsilon_{red}^k = \sum_i C_i P_i^k$.
[c]Product of $\langle P_i \rangle$ and C_i.

frequencies in addition to displacements along the normal-mode vectors. Convolution of the FCWDS spectra for oxidation of one molecule and reduction of another at a specified temperature provides the full Franck–Condon-weighted density of vibrational states, $\rho_{FC}(\Delta E, T)$, as a function of the electronic energy gap for transfer of an electron from one heme to another (Fig. 2). $\rho_{FC}(\Delta E, T)$ broadens as the temperature is increased. The calculated values of ΔE for the reactions of hemes IV and I*b* considered below fall in the region between −0.1 and +0.1 eV where $\rho_{FC}(\Delta E, T)$ increases with temperature [Fig. 2(b)].

The hemes in STC have propionyl and cysteinyl thio-ether side chains in place of four of the eight methyl groups of the model compound and histidyl residues in place of the imidazole rings. The normal modes will be more numerous in the protein, and some of the corresponding modes will have lower frequencies. However, these differences probably have only minor effects on $\rho_{FC}(\Delta E, T)$ because atoms on the periphery of a heme or its ligands are unlikely to undergo substantial displacements or changes in vibrational frequencies when the heme is oxidized or reduced. The density of states considered in Fig. 2 also does not consider vibrational modes of the protein and solvent surrounding the hemes. Although this point deserves more study, similar density distributions have been obtained from autocorrelation functions of energy gaps that included calculated interactions of the electron carriers with the surroundings.[18,46–49] The general shape of $\rho_{FC}(\Delta E)$ appears to be relatively insensitive to whether or not these interactions are included.

F. Electron-transfer matrix elements

Electronic-interaction matrix elements for electron transfer (H) were calculated by a procedure based on the PATHWAYS program described by Beratan, Onuchic, and co-workers.[50–52] Our version of the program was written to facilitate calculations of $|H|$ for a large set of structures saved during an MD trajectory and to include pathways through hydrogen atoms and water molecules as well as the

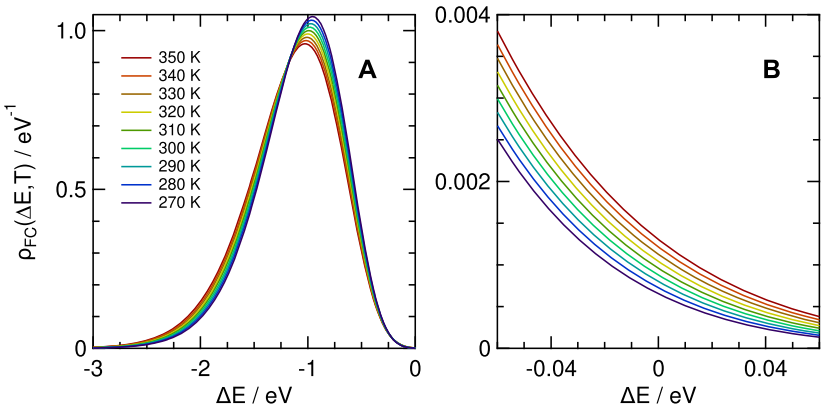

FIG. 2. Franck–Condon-weighted density of states, $\rho_{FC}(\Delta E, T)$, for transfer of an electron between two molecules of *bis*(imidazole)-iron-octamethylporphyrin at temperatures between 270 and 350 K. The abscissa (ΔE) is the instantaneous change in electronic energy, which can be converted into excitations of various combinations of vibrational normal modes or derived from thermally excited modes. The amplitude of $\rho_{FC}(\Delta E, T)$ is scaled so that $\int_{-\infty}^{\infty} \rho_{FC}(\Delta E, T) d\Delta E = 1$. Plots for $\Delta E < 0$ are shown in A, and expanded plots for the region around 0 are shown in B.

protein. The attenuation factor for transfer through a single bond was taken to be 0.6 and that for jumping between non-bonded atoms was written as $\exp[-1.7(r_{ij} - r_0)/\text{Å}]$ with $r_0 = 1.4$ Å.[50–53] To obtain absolute values, the matrix element for transfer between conjugated π atoms of a carbonyl or carboxyl group or within the ring system of a histidine, phenylalanine, tyrosine, or tryptophan residue was set at 0.1332 eV (1074 cm^{-1}), which is $1/0.6^2$ times the mean matrix element obtained by unrestricted Hartree–Fock calculations for transfer from a biphenyl radical anion through two single C–C bonds to six different acceptors in three organic solvents.[47] The calculations of H used structures recorded every 100 fs during MD trajectories in which the heme that acted as the electron donor was in its ferrous state, while all the other hemes were ferric.

The pathways program also evaluated the fluctuating "edge-to-edge" distance defined as the shortest distance from a conjugated N, C, or Fe atom of the donor heme to a conjugated N, C, or Fe atom of the acceptor.

III. RESULTS

A. Energy gaps and coupling factors for crystalline STC

Figure 3 presents calculated time-dependent energy gaps $[\Delta E(t)]$ for electron transfer from heme IV to heme I in a neighboring subunit of crystalline STC (heme I*b*), from heme I*b* back to heme IV, and from heme I*b* to II*b*. These results are from trajectories at 300 K with the electron-donor heme reduced in each case. Note, in particular, that since the identity of the reduced heme differs between the two simulations, the trace for the back reaction from heme I*b* to IV is not simply the inverse of that for transfer from IV to I*b*. The bottom panels of Fig. 3 show the calculated electronic-interaction matrix elements ($|H(t)|$) during the same trajectories. The energy gaps and the coupling matrix elements both fluctuate through relatively large deviations from the means on picosecond and nanosecond time scales. The standard deviation of $|H|$ for electron transfer from heme IV to I*b* was 35% of $\langle|H|\rangle$. For comparison, the standard deviation of the edge-to-edge distance between the two hemes was only 1.5% of the mean, indicating that the fluctuations of $|H|$ stem mainly from movements of non-conjugated atoms between the hemes rather than the hemes themselves. However, fluctuations of the edge-to-edge distance were limited partly by the constraints on the positions of the heme nitrogen atoms (see Sec. II). In MD simulations described by Kulke *et al.*,[16] which did not include such constraints, the edge-to-edge distances between hemes IV and I*b* (four pairs of hemes) at 298 K fluctuated with a standard deviation of 4.0% of the mean. The longer MD trajectories in the latter simulations also created additional opportunities for larger fluctuations of the distances to develop.

The time-dependent energy gap $\Delta E(t)$ is the sum of the change in quantum-mechanical energies of the reacting hemes and their ligands $[\Delta\varepsilon(t)]$ and the change in classical electrostatic interactions of

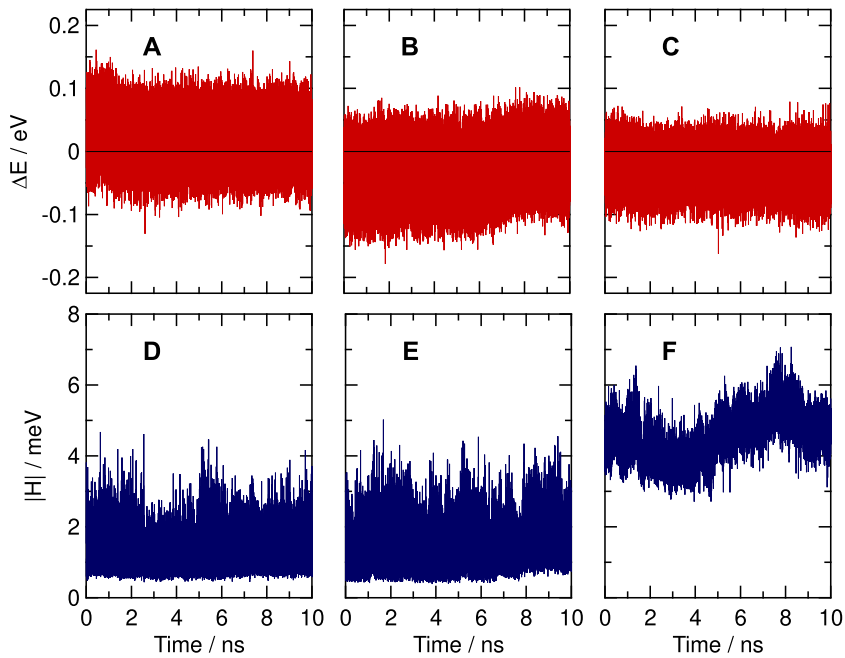

FIG. 3. Time-dependent energy gaps $[\Delta E(t)]$ calculated by Eqs. (1) and (2) for electron-transfer from heme IV to I*b* (a), heme I*b* to IV (b), and heme I*b* to II*b* (c) during MD trajectories of crystalline STC at 300 K with the electron donor reduced and the acceptor oxidized for each reaction. (d)–(f) Calculated electronic-interaction matrix elements ($|H(t)|$) for electron-transfer from heme IV to I*b*, heme I*b* to IV, and I*b* to II*b*, respectively, during the same trajectories. For the calculations of $\Delta E(t)$, carboxyl group CGA in heme IV was deprotonated (negatively charged) and CGD was protonated; CGA was protonated and CGD deprotonated in hemes I and I*b*; CGD was deprotonated and CGA protonated in hemes II and II*b*; and CGA and CGD of hemes III and III*b* were both protonated. (These are CG state 4 in Table II and state 5 in Table III.) The root-mean-square (rms) values of $|H|$ are 1.26 meV in D, 1.43 meV in E, and 4.56 meV in F.

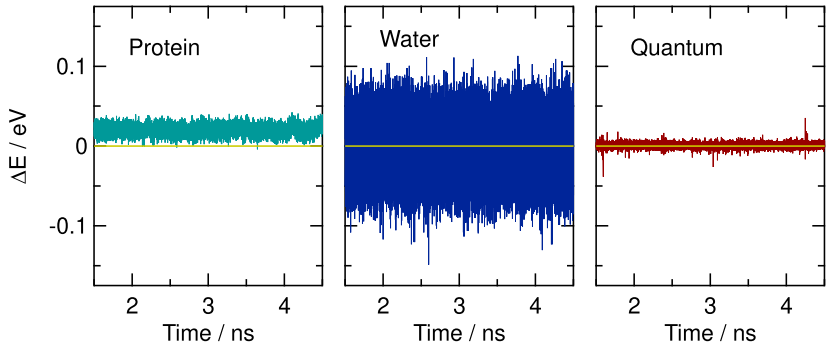

FIG. 4. Contributions of interactions with the protein (*left*) and water (*center*) and the quantum-mechanical energy difference ($\Delta\varepsilon$, *right*) to the time-dependent energy gap for electron transfer from heme IV to I*b* in crystalline STC at 300 K. These traces are representative segments of the MD trajectory shown in Fig. 3(a).

the hemes with the surrounding water and protein [$\Delta E_s(t)$]. Figure 4 shows that interactions with water make, by far, the largest contributions to the fluctuations of ΔE but have little effect on the mean value.

As noted in Sec. II, the calculated energy gaps depend on the protonation states assigned to the propionyl side chains of the electron donor and acceptor hemes. Table II gives the mean values ($\langle\Delta E\rangle$) for electron transfer between hemes IV and I*b* in STC crystals with these hemes in various protonation states. Table III presents results for electron transfer from heme I to II, which also apply to transfer from heme I*b* to II*b*. Various combinations of protonation states for the donor and acceptor hemes give values of $\langle\Delta E\rangle$ that range over about ±0.1 eV. As one would expect, a negatively charged carboxyl group on the electron donor makes electron transfer energetically more favorable, while a negatively charged group on the acceptor makes it less favorable. The protonation states of the hemes other than the electron donor and acceptor are less critical, though still significant. Deprotonating both carboxyl groups of Heme III, for example, decreased the calculated $\langle\Delta E\rangle$ for electron transfer from heme IV to I*b* by about 0.013 eV (see CG states 8–10 in Table II).

B. Energy gaps for monomeric STC in solution

Table III also gives the calculated energy gaps for electron transfer from heme I to II in monomeric STC. The values of $\langle\Delta E\rangle$ for the monomer in solution are more negative than those for the crystal

TABLE II. Effects of protonation of heme side chains on $\langle\Delta E\rangle$ and k_{et} for electron transfer between hemes IV and I*b* in crystalline STC.[a]

	Heme IV		Heme I*b*		Heme IV → I*b*		Heme I*b* → IV	
CG-state	CGA	CGD	CGA	CGD	$\langle\Delta E\rangle$/eV	$k_{4\to1b}/s^{-1}$	$\langle\Delta E\rangle$/eV	$k_{1b\to4}/s^{-1}$
1	−1	−1	0	0	−0.016 65	1.605×10^{5}	0.007 36	1.275×10^{5}
2	−1	0	0	0	−0.004 13	1.249×10^{5}	−0.005 50	1.654×10^{5}
3	−1	0	−1	0	0.017 42	7.970×10^{4}	−0.026 59	2.500×10^{5}
4	−1	0	0	−1	0.020 82	7.409×10^{4}	−0.029 95	2.666×10^{5}
5	0	0	0	−1	0.034 05	5.538×10^{4}	−0.042 03	3.329×10^{5}
6	−1	0	−1	−1	0.042 37	4.596×10^{4}	−0.051 04	3.930×10^{5}
7	0	0	−1	−1	0.055 60	3.384×10^{4}	−0.063 13	4.849×10^{5}
8	0	0	−1	−1	0.051 01	3.768×10^{4}	−0.058 70	4.488×10^{5}
9	0	0	−1	−1	0.047 20	4.110×10^{4}	−0.055 27	4.223×10^{5}
10	0	0	−1	−1	0.042 61	4.564×10^{4}	−0.050 83	3.902×10^{5}

[a]MD trajectories were propagated with the propionyl carboxyl groups of the hemes in their default protonation states (see Sec. II). Energy gaps [$\Delta E(t)$] and rate constants ($k_{4\to1b}$ and $k_{1b\to4}$), then, were calculated for electron transfer between hemes IV and I*b* in various protonation states (CG states). CGA and CGD denote the carboxyl groups of porphyrin rings A and D of the indicated hemes; −1 indicates that the group is deprotonated (negatively charged); and 0 indicates that it is protonated (neutral). See Fig. S1 for the labeling of the carboxyl groups. All the hemes other than IV and I*b* were in their default states (both carboxyl groups of hemes I, I*b*, III, and III*b* and the carboxyl groups on ring A of hemes II and II*b* and ring D of heme IV neutral; those on ring D of hemes II and II*b* and ring A of heme IV negatively charged) except that CGA of heme III was deprotonated in state 8, CGD in state 9, and both CGA and CGD in state 10. Energy gaps and rate constants were averaged over 100 000 time points during 10 ns trajectories at 300 K with the electron donor reduced and the acceptor oxidized for each reaction.

TABLE III. Effects of protonation of heme side chains on $\langle \Delta E \rangle$ and k_{et} for electron transfer from heme I to II in crystalline and monomeric STC.[a]

	Heme I		Heme II		Heme I → II in crystal		Heme I → II in monomer	
CG-state	CGA	CGD	CGA	CGD	$\langle \Delta E \rangle$/eV	$k_{1b\rightarrow 2b}/s^{-1}$	$\langle \Delta E \rangle$/eV	$k_{1\rightarrow 2}/s^{-1}$
1	0	0	0	−1	0.010 28	1.129×10^6	−0.056 16	3.765×10^6
2	0	0	0	−1	−0.005 46	1.571×10^6	−0.071 24	4.835×10^6
3	0	−1	−1	−1	−0.009 11	1.649×10^6	−0.076 39	5.252×10^6
4	−1	0	−1	−1	−0.010 00	1.726×10^6	−0.075 84	5.207×10^6
5	0	−1	0	−1	−0.026 03	2.374×10^6	−0.092 68	6.789×10^6
6	−1	0	0	−1	−0.026 91	2.416×10^6	−0.092 14	6.732×10^6
7	−1	−1	−1	−1	−0.030 57	2.596×10^6	−0.097 28	7.228×10^6
8	−1	−1	0	−1	−0.047 48	3.571×10^6	−0.113 58	9.295×10^6
9	−1	−1	0	−1	−0.046 74	3.522×10^6	−0.113 60	9.298×10^6

[a]CGA and CGD denote the carboxylic groups of porphyrin rings A and D of the indicated hemes, −1 indicates that the group is deprotonated, and 0 indicates that it is protonated. The other hemes were in their default protonation states except that CGD of heme IV in the neighboring subunit on the negative *b* axis was deprotonated in state 9. Energy gaps and electron-transfer rate constants were averaged over MD trajectories of 10 ns at 300 K with heme I reduced and II oxidized.

by 0.06–0.07 eV. Figure S4 shows that this difference stems mainly from more negative calculated energies of interactions of the hemes with the protein and to a lesser extent from the quantum term $\Delta\varepsilon$. The difference between the interactions with the protein in the crystal and the monomer probably results mainly from protein atoms of the crystal's other subunits that are not present in the monomer. The energies of interactions with water fluctuate more widely in solution than in the crystal, but again have relatively little effect on the mean value of ΔE. In crystals, movements of water are restricted to specific channels, limiting the number of thermally accessible configurations for water near the hemes. Water has greater freedom to modulate ΔE in solution.

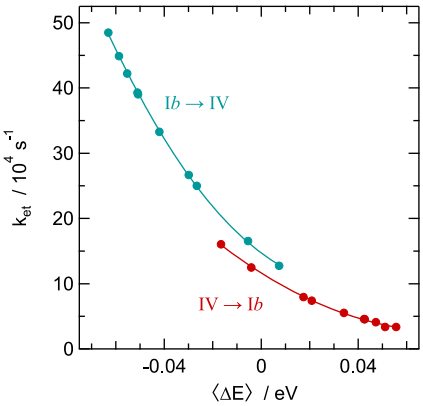

FIG. 5. Calculated rate constants for electron transfer from heme IV to I*b* ($k_{4\rightarrow 1b}$, *red*) and from heme I*b* to IV ($k_{1b\rightarrow 4}$, *cyan*) in crystalline STC at 300 K as functions of the mean energy gap between the reactant and product states. The data points represent calculations for various protonation states of the propionyl side chains of the two hemes (see Sec. II and Table II).

C. Calculated rate constants

Tables II and III present rate constants for electron transfer from heme IV to I*b* ($k_{4\rightarrow 1b}$), heme I*b* to IV ($k_{1b\rightarrow 4}$), and heme I*b* to II*b* ($k_{1b\rightarrow 2b}$), as calculated by Eq. (2) for crystalline STC at 300 K in various protonation states. Note that Eq. (2), which holds if $|H(t, T)|^2/\hbar$ is small relative to the rate constant for dissipation of energy to the surroundings, does not require knowing the exact value of the latter parameter (ξ). Although Eq. (2) does not use the mean value of the energy gap, all the rate constants increase as $\langle \Delta E \rangle$ becomes more negative. Figure 5 shows plots of $k_{4\rightarrow 1b}$ and $k_{1b\rightarrow 4}$ as functions of $\langle \Delta E \rangle$. Averaging over the broad distributions of the energy gaps (Fig. 3) makes the rate constants weaker functions of ΔE than the Franck–Condon-weighted density of states (Fig. 2). The rate constants for the backward reaction from heme I*b* to IV in crystals are higher than those for the forward reaction at similar values of $\langle \Delta E \rangle$ because the electronic coupling factor is larger in the MD trajectory with heme I*b* reduced than with heme IV reduced (Fig. 3).

Table III also gives rate constants for electron transfer from heme I to II ($k_{1\rightarrow 2}$) for monomeric STC in solution. This reaction is calculated to be about three times faster in solution than in the crystal. The higher $k_{1\rightarrow 2}$ is attributable mainly to the more negative $\langle \Delta E \rangle$ in solution (Table III and Fig. S5) because the rms value of the calculated coupling factor for the monomer (3.92 meV) is smaller than that for the crystal (4.56 meV).

Note that the rate constants in Tables II and III for STC in various protonation states use coupling factors ($|H(t)|$) and quantum mechanical energy changes ($\Delta\varepsilon$) from MD trajectories that were run in the default protonation state as described in Sec. II. We assumed that the protonation state of a propionyl side chain has only minor effects on these terms relative to its effect on ΔE_s, but this assumption remains to be tested.

One of the surprising features of electron diffusion in STC crystals is its strong dependence on temperature.[10] Figure 6 shows

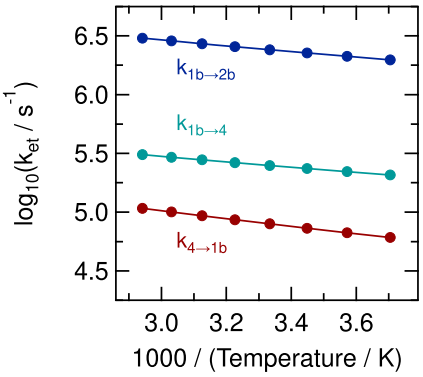

FIG. 6. Arrhenius plots of the calculated rate constants for electron transfer from heme IV to I*b* (*red*), I*b* to IV (*cyan*), and I*b* to II*b* (*dark blue*) in crystalline STC. The energy gaps and coupling factors were calculated from 10-ns trajectories at 300 K with the electron donor for each reaction reduced and the acceptor oxidized. The protonation states were the same as CG state 3 in Table II for transfer between heme IV and I*b* and CG state 6 in Table III for transfer from I*b* to II*b*. These rate constants assume that $\Delta E(t)$ is independent of temperature; their temperature dependence comes solely from $\rho_{FC}(\Delta E, T)$.

Arrhenius plots of the calculated rate constants for electron transfer from hemes IV to I*b*, I*b* to IV, and I*b* to II*b*. These calculations combine the temperature-dependent $\rho_{FC}(\Delta E, T)$ (Fig. 2) with values of the energy gaps and coupling factors from trajectories at 300 K (Figs. 3–5 and Tables II–III) on the assumption that the latter parameters are relatively insensitive to temperature. The slope of the plot for $k_{4\to 1b}$ gives an activation energy of 0.065 eV, which is about one-seventh of the value obtained in the crystal experiments (0.43 eV).[10]

Because $\rho_{FC}(\Delta E)$ has an upward curvature in the region of the mean energy gap for electron transfer from heme IV to I*b* (Fig. 2), a broadening the distribution of ΔE with increasing temperature would raise $k_{4\to 1b}$ and increase the slope of the Arrhenius plot. One might expect such broadening to result from increasing thermal fluctuations as the temperature rises. However, the variances of ΔE for electron-transfer reactions in solution often have a relatively weak dependence on temperature, probably because polar groups whose librational and vibrational motions modulate the energy gap pack more tightly around the electron carriers at lower temperatures.[11,12,54] In 5 ns MD trajectories performed at 10 K intervals between 270 and 340 K, the calculated variances of ΔE for electron transfer from heme IV to I*b* or from heme I*b* back to IV both decreased rather than increasing with temperature (Fig. S7A).

Figures S6 and S7 show that changing interactions of the electron carriers with water are responsible for the decrease in σ^2 with temperature. The variances of the quantum term ($\Delta\varepsilon$) and interactions with the protein both exhibit the more conventional behavior of increasing with temperature. In MD trajectories at various temperatures, water molecules were found to pack more tightly at particular positions near the hemes at lower temperatures. This packing gives sharper peaks in radial distribution functions of water oxygens around the Fe atoms (Fig. S8).

IV. DISCUSSION

A. Comparisons with measured rate constants

The measured rate constant for electron hopping between subunits along the crystallographic *b* axis of STC at 297 K is 7.4×10^4 s^{-1}.[10] This is expected to be somewhat smaller than the microscopic rate constant for electron transfer from heme IV to I*b* because the observed rate partly depends on the competition between electron transfer from heme I*b* to II*b* and back to heme IV [Eq. (6)],

$$\text{heme IV} \underset{k_{1b\to 4}}{\overset{k_{4\to 1b}}{\rightleftharpoons}} \text{heme I}b \xrightarrow{k_{1b\to 2b}} \text{heme II}b \rightarrow \text{hemes III}b, \text{IV}b. \tag{6}$$

(Judging from the measured reduction potentials of the hemes,[10,14] the back reaction from heme II*b* to I*b* is strongly endoergic. This reaction, therefore, is probably negligible relative to the exoergic reactions from heme I*b* to II*b* and from heme II*b* to III*b* and IV*b*.) Park[55] has given general expressions for the kinetics of reversible, sequential reactions in a system with three states. In the limit $k_{1b\to 2b} \gg k_{4\to 1b}$, which Tables II and III show to be a good approximation, the predicted time dependence of the combined population of reduced hemes II*b*, III*b*, and IV*b* [$C(t)$] simplifies to

$$C(t) = A_0\{1 - \exp[-k_{4\to 1b}t/(1 + k_{1b\to 4}/k_{1b\to 2b})]\}, \tag{7}$$

where A_0 is the concentration of reduced heme IV at time zero. The macroscopic rate constant for electron transfer between subunits along the *b* axis thus becomes $k_{4\to 1b}(1 + k_{1b\to 4}/k_{1b\to 2b})$. The calculated microscopic values of $k_{1b\to 2b}$ in crystalline STC (Table III) are about ten times the values of $k_{1b\to 4}$ in the same protonation states (Table II), mainly because the coupling factors are larger for the former reaction (Fig. 3). Competition from the back reaction from heme I*b* to IV therefore probably decreases the measured rate constant by only about 10%. Making this correction raises the estimate of $k_{4\to 1b}$ based on the experimental measurements to 8.1×10^4 s^{-1}. The calculated rate constants for CG states 3 and 4 of Table II, in which hemes IV and I*b* both have one deprotonated carboxyl group, reproduce this value well.

Experimental measurements of the rate constant for electron transfer from heme I to II in monomeric STC are problematic because the reaction does not cause a measurable change in the absorption spectrum. Van Wonderen *et al.*[56] explored the kinetics by initiating electron transfer photochemically from a Ru(II) (bipyridine)$_3$ group attached covalently to the protein near heme I and fitting the total population of charge-separated species (Ru^+Heme^-) to kinetic schemes that either included or omitted transfer between the hemes. Their schemes included multiple conformations of the Ru(II) (bipyridine)$_3$ group with different rate constants for electron transfer from Ru to the proximal heme. Van Wonderen *et al.* favored a scheme with three conformational components and an electron-transfer rate constant $k_{1\to 2}$ of 1.25×10^8 s^{-1} for all the conformations. Calculations by Jiang *et al.*[29] have given a considerably lower value of about 1.3×10^6 s^{-1} for $k_{1\to 2}$, which van Wonderen *et al.*[56] suggest could reflect an overestimate of the reorganization free energy for the reaction. However, the absorbance signals described by van Wonderen *et al.* were fit equally well by

a scheme without a significant contribution from electron transfer between the hemes if a fourth conformation of Ru(II) (bipyridine)$_3$ was included, and the possible perturbation of $k_{1\to2}$ by Ru^+ adds to the uncertainties. Our calculated k_{et} values of about 6.7×10^6 s^{-1} for monomeric STC in CG state 5 or 6 (Table III) are intermediate between the values obtained by van Wonderen *et al.*[56] and Jiang *et al.*[29] but closer to the latter.

B. Effects of temperature

The calculated activation energy of 0.065 eV for electron transfer from heme IV to I*b* (Fig. 6) is significantly smaller than the observed[10] value for electron hopping along the *b* axis in crystals. Shifting $\langle \Delta E \rangle$ to more positive values would increase the calculated value, but the calculated rate constant $k_{4\to1b}$ then would fall below the measured value unless $\langle |H| \rangle$ also was increased by a physically unrealistic degree. A more likely explanation is that, instead of decreasing as it does in our simulations, the variance of ΔE rises with temperature under the conditions that were used to measure the activation energy. The experimental measurements[10] used STC crystals suspended in 30% (*v*/*v*) polyethylene glycol 400 (PEG 400) with 0.2 M triethanolamine chloride and 5 mM $ZnSO_4$. The temperature dependence of σ^2 could be very different in that viscous medium than in simulations of crystalline STC in water since the viscosity of PEG changes steeply with temperature.[57,58] This issue takes on a broader dimension when one considers that studies of electron transfer in proteins at cryogenic temperatures almost always require viscous protectants, such as glycerol or ethylene glycol.

Another possible explanation for the failure to reproduce the measured activation energy is that fluctuations of the structure occasionally give values of $|H|$ that are substantially larger than the values seen during our simulations and that such fluctuations become more probable as the temperature rises. The present calculations of $|H|$ would miss fluctuations that occur only at intervals much longer than 10 ns. As discussed above in connection with Fig. 3, fluctuations to larger values of $|H|$ probably would mainly depend on movements of non-conjugated atoms between hemes IV and I*b* rather than changes in the edge-to-edge distance between the hemes.

Garg *et al.*[59] reported on the temperature-dependence of the electric conductivity of a dry STC monolayer sandwiched between gold electrodes. The conductivity was essentially independent of temperature between 80 and 320 K. To explain this result, Garg *et al.*[59] and Futera *et al.*[60] proposed that electron transfer occurs by coherent electron tunneling through the entire protein. However, an electron-transfer process that is independent of temperature does not necessarily imply coherent tunneling at multiple sites: it is a well-established feature of the conversion of electronic energy into excited vibrational modes.[18,49,61] Other factors being constant, the temperature dependence of $\rho_{FC}(\Delta E, T)$ vanishes at $\Delta E \approx -0.21$ and -1.15 V and is relatively small at any negative ΔE value down to about -1.5 V (Fig. 2). The energy gap for the electron-transfer step that determines the conductivity of an STC monolayer would depend on the applied potential as well as the structure of the protein in the monolayer.

Computational approaches have had notable difficulty accounting for the temperature dependence of electron conduction through nanowires of the OmcS cytochrome from *G. sulfurreductans*, which has ten *c*-type hemes in each subunit. Dahl *et al.*[62] measured currents flowing between AFM probes that contacted OmcS nanowires at various points. The conductivity increased by a factor of 100 as the temperature was lowered from 300 to 270 K. Extensive MD simulations and quantum calculations by Guberman-Pfeffer[13] were unable to reproduce this anti-Arrhenius behavior: the calculated rate constants for electron transfer were largely independent of temperature, similar to what we see in Fig. 6. Rate constants that mainly depend on the Franck–Condon-weighted density of states are expected to increase with the decreasing temperature for any $\langle \Delta E \rangle$ between about -0.21 and -1.15 V (Fig. 2), but this increase is too small to explain the observed increase of rate in OmcS if other factors are held constant.

V. CONCLUSIONS

In the treatment presented above, electron-transfer rate constants depend on the overlap of the Franck–Condon-weighted distribution of states $[\rho_{FC}(\Delta E, T)]$ with the time-dependent energy gap $\Delta E(t, T)$ and the electronic coupling factor $[|H|^2(t, T)]$. The overlap is sensitive to both the mean values and the widths of the distributions of ΔE and $|H|^2$. Calculations using this approach captured the measured rate constant for electron transfer from heme IV to I*b* at temperatures around 300 K remarkably well. However, they did not reproduce the high activation energy for electron transfer along the *b* axis of crystals. We have suggested two possible explanations for this discrepancy. Exploring these would require longer MD trajectories and simulations of systems containing a viscous cryoprotectant, which would need a long time to converge at low temperatures.

Some of the differences between our approach and MD simulations that use the semiclassical Marcus equation[19–23] have been noted in Sec. II. Perhaps the most basic difference is that Eq. (1) does not require evaluating the reorganization free energy of the reaction; it finds the rate constant from simulations of only the reactant state. Several recent papers have discussed the errors of common procedures for finding the reorganization free energy from either the variance of the energy gap ΔE or the difference between the mean values of ΔE in the reactant and product states, which stem mainly from neglecting changes in entropy.[11,12,18] By using the calculated Franck–Condon-weighted density of states, Eq. (1) also escapes the dependence on freely adjustable vibrational parameters that limits the significance of calculations using the Ultrup–Jortner[61] extension of the Marcus equation.

Figures 3 and 4 and S5–S8 highlight the importance of interactions with water in fluctuations of the energy gaps for electron transfer. Although interactions with water have little effect on the mean values of ΔE for the reactions we studied, endergonic reactions, such as the transfer of an electron from heme IV to I*b*, can depend strongly on fluctuating fields from water that make the energy gap transiently negative. Water molecules located close to the hemes probably are more important than the bulk solvent in this regard. Similar considerations would apply to endergonic steps of electron transfer in other systems, though interactions with water could affect $\langle \Delta E \rangle$ as well as σ^2 in some cases.

SUPPLEMENTARY MATERIAL

See the supplementary material for atomic charges (Table S1); Fe–N bond lengths (Table S2); labeling of heme carboxyl groups (Fig. S1); structures of heme-ligand complexes from cytochrome crystal structures (Figs. S2 and S3); structures of *bis*(imidazole)-iron-octamethylporphyrin (Fig. S4); contributions to ΔE for electron transfer from heme I to II in crystalline and monomeric STC (Fig. S5); contributions to ΔE for electron transfer from heme IV to I*b* at 270 and 340 K (Fig. S6); temperature dependences of contributions to the variance of ΔE for transfer between heme IV and I*b* (Fig. S7); and radial distributions of water around hemes IV and I*b* at 270 and 340 K (Fig. S8).

ACKNOWLEDGMENTS

D.M.K., J.V.V., and J.H. were supported by the Office of Science, Office of Basic Energy Sciences of the U.S. Department of Energy under Grant No. DE-FG02-91ER20021 and by the National Science Foundation under Award No. 1359494. This work was supported, in part, through computational resources and services provided by the Institute for Cyber-Enabled Research at Michigan State University. We thank Andrea Peluso and Amedeo Capobianco (University of Salerno) for providing MolFC3 and much helpful discussion and Clemens Burda (Case Western Reserve University) for helpful comments on the manuscript.

AUTHOR DECLARATIONS

Conflict of Interest

The authors have no conflicts to disclose.

Author Contributions

W.W.P., J.H. and D.M.K. conceptualized the study; W.W.P. performed the MD simulations and the theoretical analysis; J.V.V. and M.K. participated in the GAUSSIAN calculations of heme energies; and all the authors participated in discussing the results and preparing the manuscript.

William W. Parson: Conceptualization (equal); Formal analysis (lead); Methodology (lead); Writing – original draft (lead). **Jingcheng Huang**: Conceptualization (equal); Writing – review & editing (equal). **Martin Kulke**: Methodology (equal); Writing – review & editing (equal). **Josh V. Vermaas**: Methodology (equal); Writing – review & editing (equal). **David M. Kramer**: Conceptualization (equal); Writing – review & editing (equal).

DATA AVAILABILITY

The data that support the findings of this study are available from the corresponding author upon reasonable request.

REFERENCES

[1]D. J. Richardson, "Bacterial respiration: A flexible process for a changing environment," Microbiology **146**, 551–571 (2000).
[2]G. Reguera, K. D. McCarthy, T. Mehta, J. S. Nicoll, M. T. Tuominen, and D. R. Lovley, "Extracellular electron transfer via microbial nanowires," Nature **435**, 1098–1101 (2005).
[3]R. M. Snider, S. M. Strycharz-Glaven, S. D. Tsoi, J. S. Erickson, and L. M. Tender, "Long-range electron transport in Geobacter sulfurreducens biofilms is redox gradient-driven," Proc. Natl. Acad. Sci. U. S. A. **109**, 15467–15472 (2012).
[4]M. D. Yates, J. P. Golden, J. Roy, S. M. Strycharz-Glaven, S. Tsoi, J. S. Erickson, M. Y. El-Naggar, S. Calabrese Barton, and L. M. Tender, "Thermally activated long range electron transport in living biofilms," Phys. Chem. Chem. Phys. **17**, 32564–32570 (2015).
[5]S. Sure, M. L. Ackland, A. J. Torriero, A. Adholeya, and M. Kochar, "Microbial nanowires: An electrifying tale," Microbiology **162**, 2017–2028 (2016).
[6]S. Rengaraj, R. Haddad, E. Lojou, N. Duraffourg, M. Holzinger, A. Le Goff, and V. Forge, "Interprotein electron transfer between FeS-protein nanowires and oxygen-tolerant NiFe hydrogenase," Angew. Chem., Int. Ed. **56**, 7774–7778 (2017).
[7]D. R. Lovley and D. J. F. Walker, "Geobacter protein nanowires," Front. Microbiol. **10**, 2078 (2019).
[8]M. J. Edwards, D. J. Richardson, C. M. Paquete, and T. A. Clarke, "Role of multiheme cytochromes involved in extracellular anaerobic respiration in bacteria," Protein Sci. **29**, 830–842 (2020).
[9]S. E. Yalcin and N. S. Malvankar, "The blind men and the filament: Understanding structures and functions of microbial nanowires," Curr. Opin. Chem. Biol. **59**, 193–201 (2020).
[10]J. Huang, J. Zarzycki, M. R. Gunner, W. W. Parson, J. F. Kern, J. Yano, D. C. Ducat, and D. M. Kramer, "Mesoscopic to macroscopic electron transfer by hopping in a crystal network of cytochromes," J. Am. Chem. Soc. **142**, 10459–10467 (2020).
[11]W. W. Parson, "Reorganization energies, entropies, and free energy surfaces for electron transfer," J. Phys. Chem. B **125**, 7940–7945 (2021).
[12]W. W. Parson and C. Burda, "Calculated solvent reorganization entropies, free energies, and fluctuations of the energy gaps for intramolecular electron transfer and excitation of the solvatochromic dye B30," J. Chem. Phys. **159**, 154505 (2023).
[13]M. J. Guberman-Pfeffer, "Assessing thermal response of redox conduction for *anti*-arrhenius kinetics in a microbial cytochrome nanowire," J. Phys. Chem. B **126**, 10083–10097 (2022).
[14]E. Harada, J. Kumagai, K. Ozawa, S. Imabayashi, A. S. Tsapin, K. H. Nealson, T. E. Meyer, M. A. Cusanovich, and H. Akutsu, "A directional electron transfer regulator based on heme-chain architecture in the small tetraheme cytochrome c from *Shewanella oneidensis*," FEBS Lett. **532**, 333–337 (2002).
[15]B. M. Fonseca, I. H. Saraiva, C. M. Paquete, C. M. Soares, I. Pacheco, C. A. Salgueiro, and R. O. Louro, "The tetraheme cytochrome from Shewanella oneidensis MR-1 shows thermodynamic bias for functional specificity of the hemes," J. Biol. Inorg. Chem. **14**, 375–385 (2009).
[16]M. Kulke, D. Olson, J. Huang, D. M. Kramer, and J. Vermaas, "Long-range electron transport rates depend on wire dimensions in cytochrome nanowires," Small **19**, 2304013 (2023).
[17]A. W. McMillan, B. L. Kier, I. Shu, A. Byrne, N. H. Andersen, and W. Parson, "Fluorescence of tryptophan in designed hairpin and Trp-cage miniproteins: Measurements of fluorescence yields and calculations by quantum mechanical molecular dynamics simulations," J. Phys. Chem. B **117**, 1790–1809 (2013).
[18]W. W. Parson, "Generalizing the Marcus equation," J. Chem. Phys. **152**, 184106 (2020).
[19]R. A. Marcus, "Free energy of nonequilibrium polarization systems. III. Statistical mechanics of homogeneous and electrode systems," J. Chem. Phys. **39**, 1734–1740 (1963).
[20]R. A. Marcus, "On the theory of electron-transfer reactions. VI. Unified treatment for homogeneous and electrode reactions," J. Chem. Phys. **43**, 679–701 (1965).

[21]R. A. Marcus and N. Sutin, "Electron transfers in chemistry and biology," Biochim. Biophys. Acta, Rev. Bioenerg. **811**, 265–322 (1985).
[22]D. V. Matyushov, "Energetics of electron-transfer reactions in soft condensed media," Acc. Chem. Res. **40**, 294–301 (2007).
[23]S. Seyedi and D. V. Matyushov, "Termination of biological function at low temperatures: Glass or structural transition," J. Phys. Chem. Lett. **9**, 2359–2366 (2018).
[24]D. Leys, T. E. Meyer, A. S. Tsapin, K. H. Nealson, M. A. Cusanovich, and J. J. Van Beeumen, "Crystal structures at atomic resolution reveal the novel concept of "electron-harvesting" as a role for the small tetraheme cytochrome c," J. Biol. Chem. **277**, 35703–35711 (2002).
[25]G. King and A. Warshel, "A surface constrained all-atom solvent model for effective simulations of polar solutions," J. Chem. Phys. **91**, 3647–3661 (1989).
[26]F. S. Lee, Z. T. Chu, and A. Warshel, "Microscopic and semimicroscopic calculations of electrostatic energies in proteins by the POLARIS and ENZYMIX programs," J. Comput. Chem. **14**, 161–185 (1993).
[27]W. W. Parson and A. Warshel, in *Biophysical Techniques in Photosynthesis*, edited by T. J. Aartsma and J. Matysik (Springer, Dordrecht, The Netherlands, 2008), pp. 401–420.
[28]A. S. F. Oliveira, V. H. Teixeira, A. M. Baptista, and C. M. Soares, "Reorganization and conformational changes in the reduction of tetraheme cytochromes," Biophys. J. **89**, 3919–3930 (2005).
[29]X. Jiang, Z. Futera, M. E. Ali, F. Gajdos, G. F. vonRudorff, A. Carof, M. Breuer, and J. Blumberger, "Cysteine linkages accelerate electron flow through tetra-heme protein STC," J. Am. Chem. Soc. **139**, 17237–17240 (2017).
[30]D. R. Martin and D. V. Matyushov, "Non-Gaussian statistics and nanosecond dynamics of electrostatic fluctuations affecting optical transitions in proteins," J. Phys. Chem. B **116**, 10294–10300 (2012).
[31]Z. Futera, X. Jiang, and J. Blumberger, "Ergodicity breaking in thermal biological electron transfer? Cytochrome c revisited II," J. Phys. Chem. B **124**, 3336–3342 (2020).
[32]A. Warshel and M. Levitt, "Theoretical studies of enzymic reactions: Dielectric, electrostatic and steric stabilization of the carbonium ion in the reaction of lysozyme," J. Mol. Biol. **103**, 227–249 (1976).
[33]A. Warshel, S. T. Russell, and A. K. Churg, "Macroscopic models for studies of electrostatic interactions in proteins: Limitations and applicability," Proc. Natl. Acad. Sci. U. S. A. **81**, 4785–4789 (1984).
[34]E. T. Johnson and W. W. Parson, "Electrostatic interactions in an integral membrane protein," Biochemistry **41**, 6483–6494 (2002).
[35]A. Warshel, P. K. Sharma, M. Kato, and W. W. Parson, "Modeling electrostatic effects in proteins," Biochim. Biophys. Acta, Proteins Proteomics **1764**, 1647–1676 (2006).
[36]E. L. Rothery, C. G. Mowat, C. S. Miles, S. Mott, M. D. Walkinshaw, G. A. Reid, and S. K. Chapman, "Probing domain mobility in a flavocytochrome," Biochemistry **43**, 4983–4989 (2004).
[37]I. Bento, P. M. Matias, A. M. Baptista, P. N. Da Costa, W. M. A. M. van Dongen, L. M. Saraiva, T. R. Schneider, C. M. Soares, and M. A. Carrondo, "Molecular basis for redox Bohr and cooperative effects in cytochrome c_3 from *Desulfovibrio desulfuricans* ATCC 27774: Crystallographic and modeling studies of oxidized and reduced high-resolution structures at pH 7.6," Proteins: Struct., Funct., Bioinf. **54**, 135–152 (2004).
[38]M. V. Pattarkine, J. J. Tanner, C. A. Bottoms, Y. H. Lee, and J. D. Wall, "Desulfovibrio desulfuricans G20 tetraheme cytochrome structure at 1.5 Å and cytochrome interaction with metal complexes," J. Mol. Biol. **358**, 1314–1327 (2006).
[39]Y. Takayama, N. D. Werbeck, H. Komori, K. Morita, K. Ozawa, Y. Higuchi, and H. Akutsu, "Strategic roles of axial histidines in structure formation and redox regulation of tetraheme cytochrome *c*3," Biochemistry **47**, 9405–9415 (2008).
[40]F. Wang, Y. Gu, J. P. O'Brien, S. M. Yi, S. E. Yalcin, V. Srikanth, C. Shen, D. Vu, N. L. Ing, A. L. Hochbaum, E. H. Egelman, and N. S. Malvankar, "Structure of microbial nanowires reveals stacked hemes that transport electrons over micrometers," Cell **177**, 361–369.e10 (2019).
[41]M. J. Frisch, G. W. Trucks, H. B. Schlegel, G. E. Scuseria, M. A. Robb, J. R. Cheeseman, G. Scalmani, V. Barone, G. A. Petersson, H. Nakatsuji, X. Li, M. Caricato, A. V. Marenich, J. Bloino, B. G. Janesko, R. Gomperts, B. Mennucci, H. P. Hratchian, J. V. Ortiz, A. F. Izmaylov, J. L. Sonnenberg, D. Williams-Young, F. Ding, F. Lipparini, F. Egidi, J. Goings, B. Peng, A. Petrone, T. Henderson, D. Ranasinghe, V. G. Zakrzewski, J. Gao, N. Rega, G. Zheng, W. Liang, M. Hada, M. Ehara, K. Toyota, R. Fukuda, J. Hasegawa, M. Ishida, T. Nakajima, Y. Honda, O. Kitao, H. Nakai, T. Vreven, K. Throssell, J. A. Montgomery, Jr., J. E. Peralta, F. Ogliaro, M. J. Bearpark, J. J. Heyd, E. N. Brothers, K. N. Kudin, V. N. Staroverov, T. A. Keith, R. Kobayashi, J. Normand, K. Raghavachari, A. P. Rendell, J. C. Burant, S. S. Iyengar, J. Tomasi, M. Cossi, J. M. Millam, M. Klene, C. Adamo, R. Cammi, J. W. Ochterski, R. L. Martin, K. Morokuma, O. Farkas, J. B. Foresman, and D. J. Fox, *GAUSSIAN 16, Revision B.01*, Gaussian, Inc., Wallingford CT, 2016.
[42]D. M. A. Smith, M. Dupuis, E. R. Vorpagel, and T. P. Straatsma, "Characterization of electronic structure and properties of a bis(histidine) heme model complex," J. Am. Chem. Soc. **125**, 2711–2717 (2003).
[43]R. Borrelli and A. Peluso, "Dynamics of radiationless transitions in large molecular systems: A Franck–Condon-based method accounting for displacements and rotations of all the normal coordinates," J. Chem. Phys. **119**, 8437–8448 (2003).
[44]R. Borrelli, A. Capobianco, and A. Peluso, "Generating function approach to the calculation of spectral band shapes of free-base chlorin including Duschinsky and Herzberg-Teller effects," J. Phys. Chem. A **116**, 9934–9940 (2012).
[45]R. Borrelli, A. Capobianco, and A. Peluso, "Franck–Condon factors. Computational approaches and recent developments," Can. J. Chem. **91**, 495–505 (2013).
[46]W. W. Parson, "Vibrational relaxations and dephasing in electron-transfer reactions," J. Phys. Chem. B **120**, 11412–11418 (2016).
[47]W. W. Parson, "Effects of free energy and solvent on rates of intramolecular electron transfer in organic radical anions," J. Phys. Chem. A **121**, 7297–7306 (2017).
[48]W. W. Parson, "Electron-transfer dynamics in a Zn-porphyrin-quinone cyclophane: Effects of solvent, vibrational relaxations, and conical intersections," J. Phys. Chem. B **122**, 3854–3863 (2018).
[49]W. W. Parson, "Temperature dependence of the rate of intramolecular electron transfer," J. Phys. Chem. B **122**, 8824–8833 (2018).
[50]D. N. Beratan, J. N. Betts, and J. N. Onuchic, "Protein electron transfer rates set by the bridging secondary and tertiary structure," Science **252**, 1285–1288 (1991).
[51]D. N. Beratan, J. N. Onuchic, J. R. Winkler, and H. B. Gray, "Electron-tunneling pathways in oroteins," Science **258**, 1740–1741 (1992).
[52]D. N. Beratan and J. N. Onuchic, in *Protein Electron Transfer*, edited by D. S. Bendall (BIOS Scientific Publishers, Oxford, 1996), pp. 23–42.
[53]A. de la Lande and D. R. Salahub, "Derivation of interpretative models for long range electron transfer from constrained density functional theory," J. Mol. Struct.: THEOCHEM **943**, 115–120 (2010).
[54]K. Echelberry, H. Burda, P. Willis, W. W. Parson, and C. Burda, "Temperature-dependent solvent reorganization entropies, free energies, and transition dipole strengths for the photoexcitation of Reichardt's dye B30," J. Chem. Phys. **159**, 154506 (2023).
[55]T. J. Park, "Kinetics of reversible consecutive reactions," Bull. Korean Chem. Soc. **34**, 243–245 (2013).
[56]J. H. van Wonderen, C. R. Hall, X. Jiang, K. Adamczyk, A. Carof, I. Heisler, S. E. H. Piper, T. A. Clarke, N. J. Watmough, I. V. Sazanovich, M. Towrie, S. R. Meech, J. Blumberger, and J. N. Butt, "Ultrafast light-driven electron transfer in a Ru(II)tris(bipyridine)-labeled multiheme cytochrome," J. Am. Chem. Soc. **141**, 15190–15200 (2019).
[57]M. A. Marcos, D. Cabaleiro, M. J. G. Guimarey, M. J. P. Comunas, L. Fedele, J. Fernandez, and L. Lugo, "PEG 400-based phase change materials nano-enhanced with functionalized graphene nanoplatelets," Nanomaterials **8**, 16 (2017).
[58]M. C. M. Sequeira, M. F. V. Pereira, H. M. N. T. Avelino, F. J. P. Caetano, and J. M. N. A. Fareleira, "Viscosity measurements of poly(ethyleneglycol) 400 [PEG 400] at temperatures from 293 K to 348 K and at pressures up to 50 MPa using the vibrating wire technique," Fluid Phase Equilib. **496**, 7–16 (2019).
[59]K. Garg, M. Ghosh, T. Eliash, J. H. van Wonderen, J. N. Butt, L. Shi, X. Jiang, F. Zdenek, J. Blumberger, I. Pecht, M. Sheves, and D. Cahen, "Direct evidence for heme-assisted solid-state electronic conduction in multi-heme *c*-type cytochromes," Chem. Sci. **9**, 7304–7310 (2018).
[60]Z. Futera, I. Ide, B. Kayser, K. Garg, X. Jiang, J. H. van Wonderen, J. N. Butt, H. Ishii, I. Pecht, M. Sheves, D. Cahen, and J. Blumberger, "Coherent electron

transport across a 3 nm bioelectronic junction made of multi-heme proteins," J. Phys. Chem. Lett. **11**, 9766–9774 (2020).
[61] J. Ulstrup and J. Jortner, "The effect of intramolecular quantum modes on free energy relationships for electron transfer reactions," J. Chem. Phys. **63**, 4358–4368 (1975).
[62] P. J. Dahl, S. M. Yi, Y. Gu, A. Acharya, C. Shipps, J. Neu, J. P. O'Brien, U. N. Morzan, S. Chaudhuri, M. J. Guberman-Pfeffer, D. Vu, S. E. Yalcin, V. S. Batista, and N. S. Malvankar, "A 300-fold conductivity increase in microbial cytochrome nanowires due to temperature-induced restructuring of hydrogen bonding networks," Sci. Adv. **8**(19), eabm7193 (2022).